Astronomy & Astrophysics manuscript no. Paper_compl_DLA_FINAL_version_two_col
March 7, 2024
©ESO 2024

Multiple origins for the DLA at $z_{\rm abs} = 0.313$ toward PKS 1127−145 indicated by a complex dust depletion pattern of Ca, Ti, and Mn

C. R. Guber[1], P. Richter[1,2], and M. Wendt[1]

[1] Institut für Physik und Astronomie, Universität Potsdam, Karl-Liebknecht-Str. 24/25, 14476 Golm, Germany
[2] Leibniz-Institut für Astrophysik Potsdam (AIP), An der Sternwarte 16, 14482 Potsdam, Germany

Received xxx; accepted xxx

arXiv:1709.07030v1 [astro-ph.GA] 20 Sep 2017

ABSTRACT

Aims. We aim to investigate the dust depletion properties of optically thick gas in and around galaxies and its origin we study in detail the dust depletion patterns of Ti, Mn, and Ca in the multi-component damped Lymanα (DLA) absorber at $z_{\rm abs} = 0.313$ toward the quasar PKS 1127−145.
Methods. We performed a detailed spectral analysis of the absorption profiles of Ca II, Mn II, Ti II, and Na I associated with the DLA toward PKS 1127−145, based on optical high-resolution data obtained with the UVES instrument at the Very Large Telescope (VLT). We obtained column densities and Doppler-parameters for the ions listed above and determine their gas-phase abundances, from which we conclude on their dust depletion properties. We compared the Ca and Ti depletion properties of this DLA with that of other DLAs.
Results. One of the six analyzed absorption components (component 3) shows a striking underabundance of Ti and Mn in the gas-phase, indicating the effect of dust depletion for these elements and a locally enhanced dust-to-gas ratio. In this DLA and in other similar absorbers, the Mn II abundance follows that of Ti II very closely, implying that both ions are equally sensitive to the dust depletion effects.
Conclusions. Our analysis indicates that the DLA toward PKS 1127−145 has multiple origins. With its narrow line width and its strong dust depletion, component 3 points toward the presence of a neutral gas disk from a faint LSB galaxy in front of PKS 1127−145, while the other, more diffuse and dust-poor, absorption components possibly are related to tidal gas features from the interaction between the various, optically confirmed galaxy-group members. In general, the Mn/Ca II ratio in sub-DLAs and DLAs possibly serves as an important indicator to discriminate between dust-rich and dust-poor in neutral gas in and around galaxies.

Key words. quasars: absorption lines, PKS 1127−145 – dust, extinction – galaxies: abundances – galaxies: ISM – intergalactic medium, kinematics and dynamics.

1. Introduction

Quasar absorption spectroscopy is a powerful method to study diffuse gas inside and outside of galaxies in the local Universe as well as at high redshift. This method provides accurate information about the distribution, the chemical composition, and the kinematics of the interstellar, circumgalactic, and intergalactic medium at low and high redshift (ISM, CGM, IGM, respectively; e.g., Bahcall & Spitzer 1969; Bergeron 1986; Morris et al. (1993); Savage et al. (2002)).

Most of the diagnostic transitions for quasar (or QSO) absorption spectroscopy from the most abundant atoms and ions (e.g., H I, O I, C IV, Si III, Mg II) are located in the ultraviolet (UV) at wavelengths < 2000 Å (see Morton 2003). The observation of these transitions at low redshift requires a space-based UV spectrograph, such as the Cosmic Origins Spectrograph (COS) on board the *Hubble Space Telescope* (HST). However, a few strong transitions from, if at all, only few times ionized ions of relatively abundant elements (e.g., Ca II, Ti II, Mn II, Na I) are present also in the near-UV and optical regime. In the low-z Universe, these transitions can be observed using high-resolution ground-based spectrographs at 8 m-class telescopes (e.g., the UVES instrument at the Very Large Telescope, VLT).

Intervening QSO absorbers with the highest neutral gas column densities are referred to as damped Lymanα absorbers (DLAs; $\log N(\mathrm{H\,I}) \geq 20.3$) and sub-DLAs ($19.0 \leq \log N(\mathrm{H\,I}) < 20.3$). These systems are believed to arise in a broad range of galactic and circumgalactic environments (e.g., neutral gas disks of late-type galaxies, interstellar gas in dwarf galaxies, cold gas in accretion flows, tidal gas streams from interacting galaxies). Disentangling these different origins for individual systems requires supplementary imaging data (to study the local galaxy environment) and (ideally) some other kind of information (e.g., from radio and infrared observations).

Previous absorption-line studies of DLAs and sub-DLAs have provided a wealth of information on gas-phase abundances (e.g., Dessauges-Zavadsky et al. 2006), absorber kinematics (e.g., Rao et al. 2011), overall dust properties in the absorbers (e.g., De Cia et al. 2013), and intrinsic dust

Send offprint requests to: C. R. Guber
e-mail: guber@astro.physik.uni-potsdam.de

depletion patterns (e.g., De Cia et al. 2016; Ledoux, Bergeron & Petitjean 2002; Ledoux, Petitjean & Srianand 2003) that can be derived from high-resolution spectra. However, although there are also studies concerning Ca II and Ti II absorption (e.g., Ledoux, Bergeron & Petitjean 2002; Richter et al. 2011; Welty & Crowther 2010), little attention has been paid to the ratio of these two extremely dust-affine elements. In our previous paper, Guber & Richter (2016), we have carried out a systematic study of dust depletion in DLAs and sub-DLAs using the Ca II and Ti II transitions and the ratio of these ions in the near-UV and optical regime.

According to each of their ionization potentials in predominantly neutral gas, Ti and Mn are particularly present in the form of their one-times ionized ions Ti II and Mn II, measured by us. Because the ionization potential of Ca II is slightly smaller than that of H I, also the second times ionized Ca-ion (Ca III) may contribute remarkably to the total Ca abundance in such neutral environments (e.g., Guber & Richter 2016). Unfortunately, Ca III is not spectroscopically measurable in our study. To express the fact that we know and use only the Ca II column densities for calculations, and not those of Ca III, we explicitly write [Ca II/H], Ti/Ca II, Mn/Ca II, [Ti/Ca II], and [Mn/Ca II] in the following.

Although statistics do not necessarily exclude a more continuous distribution, our study indicates that there are two distinct populations of sub-DLAs/DLAs with either high or low Ti/Ca II ratios separated at [Ti/Ca II] $\simeq 1.0$, reflecting the local dust depletion properties. We find that Ca generally tends to deplete severely in neutral gas that contains Ca and other metals while strong Ti depletion is present only in relatively dust-rich environments. The observed trends suggest that absorbers with high Ti/Ca II ratios have dust-to-gas ratios that are substantially lower than in the Milky Way and that the observed Ti/Ca II ratio represents a useful measure for the local dust-to-gas ratio in QSO absorbers.

In our initial survey (Guber & Richter 2016) we have studied integrated (averaged) Ti/Ca II ratios in a large sample of low- and high-redshift absorbers because most of these systems exhibit three or less individual absorption components in Ca and Ti. Here, we continue our systematic analysis of Ti/Ca II ratios in DLAs and sub-DLAs by studying intrinsic variations of Ti/Ca II in a single DLA system at $z = 0.313$ toward PKS 1127−145 (J113007−144927) that is characterized by at least six individual (well-separated) velocity components in Ca II and Ti II.

In the following, we label the overall DLA system (which consists of at least six components) with the term "DLA", while we write "component of the DLA" when we address one of its components.

The primary goal of our study is to investigate (and separate by their dust content) the different neutral gas phases in the overall galaxy environment that give rise to this particular absorption system. Next to Ti, Ca, and Na, we also study intrinsic variations of Mn absorption in this DLA and compare the trends for Mn/Ca II with other DLAs at low- and high-redshift.

This paper is structured as follows. In Sect. 2, we briefly summarize the previously known properties of the DLA at $z = 0.313$ toward PKS 1127−145, as derived from the many previous studies of this absorber. In Sect. 3, we outline the data reduction of our VLT/UVES data and present the analysis method. In Sect. 4, we discuss the multiple origins of the DLA sub-components in the light of their dust depletion properties. A more general discussion of the use of the Mn/Ca II ratio as potential dust indicator in DLAs and sub-DLAs is provided in Sect. 5. Finally, we summarize our study in Sect. 6.

2. The DLA at $z = 0.313$ toward PKS 1127−145

The DLA at $z = 0.313$ toward the quasar PKS 1127−145 ($z_{\rm em} = 1.18$) belongs to the best-studied low-redshift DLAs in the literature (e.g., Bergeron & Boissé 1991; Guillemin 1997; Lane et al. 1998; Rao & Turnshek 2000; Chengalur & Kanekar 2000; Nestor et al. 2002; Rao et al. 2003; Chen & Lanzetta 2003; Chun et al. 2006; Nerayanan al. 2007; Kanekar et al. 2009; Kacprzak, Murphy & Churchill 2010; Kacprzak et al. 2010; Richter et al. 2011; Guber & Richter 2016). There is a very rich data set for this DLA based on various different observatories including high-resolution, high S/N optical spectra from VLT/UVES, low-resolution UV spectral data from HST/STIS and HST/FOS, H I 21 cm absorption spectra, as well as deep optical imaging (e.g., from HST/WFPC-2) and spectral data for the nearby galaxy population.

The DLA at $z = 0.313$ toward PKS 1127−145 is characterized by a large neutral hydrogen column density ($\log N({\rm H\,I}) = 21.71$; Lane et al. 1998; Rao & Turnshek 2000) and a complex pattern of at least six individual absorption components in Mg II that span a velocity range of $\sim 380\,{\rm km\,s^{-1}}$ (Kacprzak, Murphy & Churchill 2010; Richter et al. 2011), a range that is far too large to be explained by a simple rotating gas disk. From the extensive study of Kacprzak et al. (2010) follows that the DLA is connected with a group of at last five galaxies at $z_{\rm abs} = 0.3$ with B-band luminosities in the range $(0.04-0.63)\,L_B^\star$ and sightline impact parameters $\rho/\,{\rm kpc} \in [17-241]$. However, it remains unclear which of these galaxies (if any) is responsible for the observed strong DLA. Kacprzak, Murphy & Churchill (2010) favor a scenario in which the absorption is caused by tidal debris from a recent merger event in the galaxy group.

The overall metallicity of the DLA has been constrained to ∼0.13 solar based on the Zn II/H I ratio in the gas (Kanekar et al. 2009). Interestingly, this abundance is four to ten times lower than the metallicity of the five candidate host galaxies (Kacprzak et al. 2010). If one takes the observed radial metallicity gradients in DLAs and galaxies into account (e.g., Christensen et al. 2014, Pilyugin, Grebel & Kniazev 2014, Pilyugin et al. 2014), the low metal abundance in the absorber could be explained by gas that resides in the outer regions in one of the five candidate galaxies, far away from the central star-forming regions (e.g., in the outer gas disk or in a metal-poor accretion flow). Alternatively, the DLA system might be connected with a low-surface brightness (LSB) galaxy, as suggested by Rao et al. (2003) to explain several low surface-brightness emission features close to the quasar. The various H I 21 cm absorption features detected in the DLA (Chengalur & Kanekar 2000) are co-aligned in velocity with the Ca II absorption (Richter et al. 2011) tracing the cold neutral gas component in the absorber. Yet, the average spin temperature derived from the 21 cm data is $T_{\rm spin} = (910 \pm 160)$ K, thus relatively high compared to other DLAs with large velocity spreads (see survey by Chengalur & Kanekar 2000). This possibly

suggests that much of the H I is warm, as expected for tidal streams (e.g., Brüns et al. 2003).

In this paper, we further investigate the nature of the gas in the DLA by considering the dust depletion properties in the individual velocity components.

3. Data origin and analysis method

The high resolution data for PKS 1127−145 were taken with the Ultraviolet and Visual Echelle Spectrograph (UVES) mounted on the 8.2 m Very Large Telescope (VLT) at Paranal, Chile (Dekker et al. 2010).

The slit width of 1.0 arcsec and a charge-coupled device (CCD) readout with 2×2 binning used for all the observations resulted in a spectral resolution power R ≈ 45,000, corresponding to ∼6.7 km s^{-1}, while the S/N is ≈100 at 3934 Å near the redshifted Ca II absorption.

To cover the wavelength range of the (redshifted) Na I D1 and D2 lines as well, we combined data of three different observation programs publicly available in the ESO archive[1]. The details of the observational campaigns are presented in Table A.1.

The Common Pipeline Language (CPL version 6.3) of the UVES pipeline was used to bias correct and flat field the exposures and then to extract the wavelength calibrated flux. After the standard reduction, the custom software UVES popler[2] (version 0.66) was used to combine the extracted echelle orders into single 1D spectra. The continuum was fitted with low-order polynomials.

The other UVES data used in Sect. 5 are taken from our previous survey papers (Richter et al. (2011); Guber & Richter (2016)). These raw data were reduced as part of the SQUAD project (PI: M. Murphy) with a comparable S/N and resolution as for PKS 1127−145.

In Fig. A.1, we show the velocity profiles of several transitions from Ca II, Ti II, and Mn II. In part due to a lack of spectral coverage, no diffuse interstellar bands (DIBs) associated with the DLA could be identified by us in the UVES spectra.

For the spectral analysis, we used the `fitlyman`-tool in MIDAS to fit Voigt-profiles to the individual velocity components of Ca II and created a component template. We then fixed the redshifts of the individual components and, using that template, fitted Voigt-profiles also to the other ions considered here (Ti II, Mn II, and Na I). For Na I, we allowed `fitlyman` to vary the component's centroid velocity within 2 km s^{-1} from the fixed ones of the other ions to account for the possibility that Na I traces a slightly different (more dense) gas phase than the other above mentioned ions (see Table 1). The Doppler parameters b were allowed to vary independently for each fitted ion, but were fixed for all transitions of the same ion. Table A.2 in the Appendix lists the vacuum-wavelengths and oscillator strengths of the transitions that were fitted by us. To roughly estimate the H I column densities in each component, we adopted the overall H I column density of the DLA of $\log N({\rm H\,I}) = 21.71$ (Lane et al. 1998; Rao et al. 2003) and calculated the fractional abundance of H I per component from the observed Ca II column density pattern (i.e., we assume a constant Ca II/H I ratio throughout the DLA as a first-order approximate).

[1] 67.A-0567(A), 69.A-0371(A), 076.A-0860(A)

[2] `http://astronomy.swin.edu.au/~mmurphy/UVES_popler/`

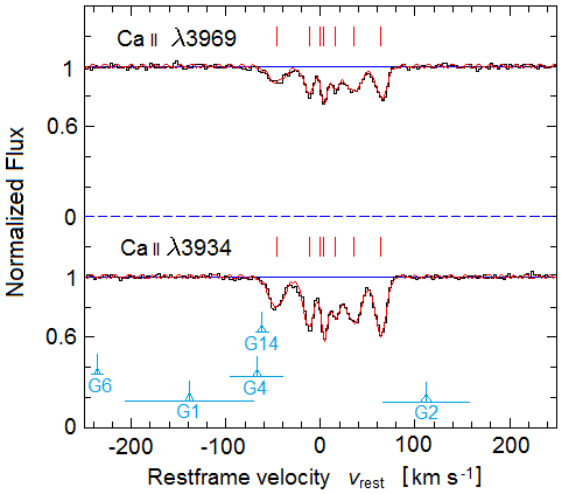


Fig. 1. Velocity profiles of Ca II λ3934, 3969 absorption in the DLA at $z_{\rm abs} = 0.312710$ toward PKS 1127−145. The velocities of the five galaxies belonging to the galaxy-group at $z_{\rm abs} = 0.313$ along the PKS 1127−145 sightline (Kacprzak et al. 2010) are indicated in blue. The horizontal lines indicate the velocity range allowed for the individual galaxies based on a simple disk-rotation scheme for these galaxies (Kacprzak, Murphy & Churchill 2010).

We presupposed solar relative abundances given in Asplund et al. (2009) and a standard ΛCDM-cosmology with $H_0 = 70\,{\rm km\,s^{-1}\,Mpc^{-1}}$, $\Omega_{\rm M} = 0.3$, and $\Omega_\Lambda = 0.7$ in accordance with Kacprzak, Murphy & Churchill (2010). All column densities $N[{\rm cm^{-2}}]$ are given in logarithmic units.

4. Origin of gas in the DLA at $z_{\rm abs} = 0.313$ toward PKS 1127−145

4.1. Component structure and galaxy environment

In Fig. 1, we show the Ca II velocity-component structure of the DLA toward PKS 1127−145 as seen in our UVES data together with the best Voigt-profile fit. Six absorption components are identified (see Table 1). In the lower panel of Fig. 1, we also show the velocities of nearby galaxies (G), as identified in the detailed study of Kacprzak, Murphy & Churchill (2010). In this figure, we indicate the velocity range allowed for the individual galaxies based on a simple disk-rotation scheme for these galaxies (Kacprzak, Murphy & Churchill 2010). Kacprzak, Murphy & Churchill (2010) identify five galaxies belonging to the same group of galaxies that all have redshifts $z_{\rm abs} \approx 0.313$. Their galaxy "G1" is the one with the smallest angular distance to the quasar sightline (3.81 arcsec, corresponding to 17.4 kpc at this redshift). However, in view of the observed velocity pattern of the galaxies and the absorber, a clear correlation between these five galaxies and the DLA components is not evident. The spatial position of the galaxies in the quasar field is sketched in Fig. 2, based on the galaxy data presented in Kacprzak, Murphy & Churchill (2010).

4.2. Gas phases abundances in the individual components

In Table 1, we list the column densities and Doppler-parameters b for the individual velocity components derived from our Voigt-profile fitting. The measured Ca II column

Table 1. Results from the Voigt-profile fitting of the six components in the DLA at $z_{\rm abs} = 0.313$ toward PKS 1127−145. The velocities are given in the $z = 0.312710$ restframe, as assumed by Kacprzak, Murphy & Churchill (2010). For Na I, we allowed `fitlyman` to vary the component's centroid velocity within $2\,{\rm km\,s^{-1}}$ from the fixed values for the other ions. The values in brackets in column two are these slightly deviant velocities of the components in Na I. The upper limits for N(Na I) were derived from the signal-to-noise ratio without the need for specific component-velocities. The Doppler-parameters b are from the fits of the Ca II lines. For the H I column densities, a proportionality between the column densities of Ca II- & H I and an overall H I column density of $\log N({\rm H\,I}) = 21.71$ are assumed.

Comp.	$v_{\rm rest}$ $[{\rm km\,s^{-1}}]$	b (Ca II) $[{\rm km\,s^{-1}}]$	$\log N$(H I)	$\log N$(Ca II)	$\log N$(Ti II)	$\log N$(Mn II)	$\log N$(Na I)
1	−46.5	11.2	20.97	11.85±0.01	11.96±0.03	12.44±0.02	<11.21
2	−12.3 (−11.25)	6.8	21.04	11.92±0.01	12.37±0.02	12.72±0.01	12.28±0.07
3	+4.0 (+2.31)	2.6	20.99	11.87±0.01	(10.12±1.08)[a]	11.09±0.16	11.93±0.04
4	+15.6 (+15.88)	5.8	20.88	11.76±0.02	11.78±0.07	12.16±0.03	11.89±0.05
5	+35.3	10.6	21.17	12.05±0.01	12.07±0.03	12.56±0.01	<11.21
6	+64.4	6.8	21.14	12.02±0.01	11.84±0.04	12.09±0.02	<11.21
total	–	–	21.71	12.59±0.02	12.76±0.04	13.16±0.02	$12.55^{+0.11}_{-0.06}$

Notes. (a) Only weakly constrained; no impact on total budget.

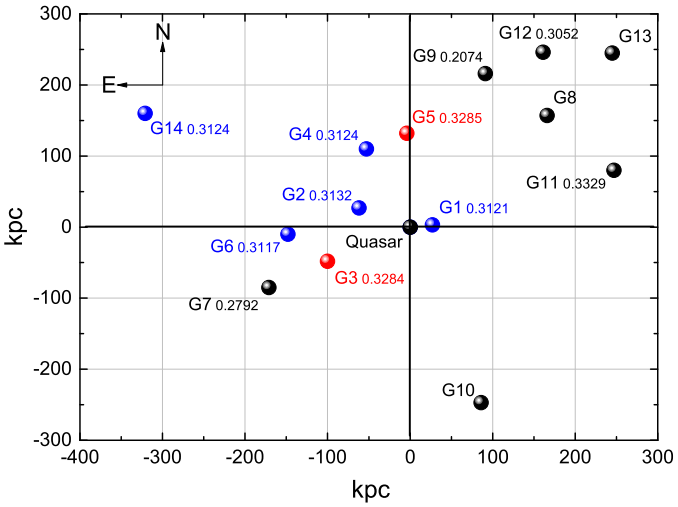


Fig. 2. Absorber-galaxy connection for the DLA toward PKS 1127−145 at $z_{\rm abs} = 0.313$ (adopted from Kacprzak et al. 2010).

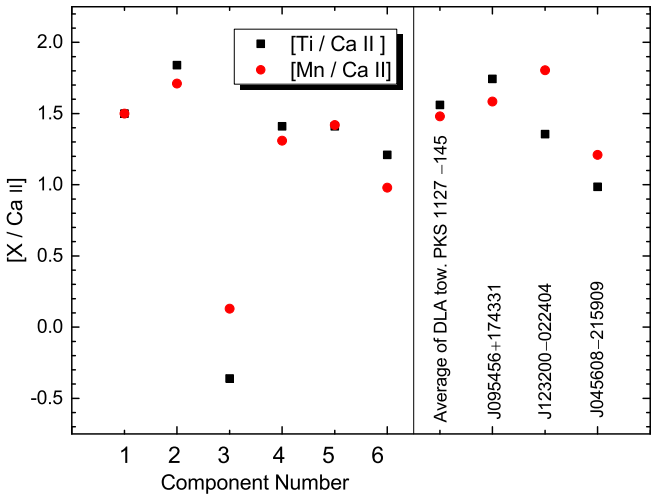


Fig. 3. Gas-phase abundances [X/Ca II] for X=Ti and X=Mn for the six components in the DLA toward PKS 1127−145 and other DLAs and sub-DLAs from the Guber & Richter (2016) absorber sample (see also Table A.3).

densities lie all within a small range, $\log N \in [11.76, 12.02]$. For Ti II and Mn II, in contrast, the dispersion is larger, since the column densities in component 3 are substantially smaller than in the other components (see Table 1). We note at this point that each of the absorption components would be a DLA on its own if observed as a single absorption system (see H I column densities for the individual components in Table 1, fourth column).

In Fig. 3, we plot the abundance ratios [Ti/Ca II] and [Mn/Ca II] based on the adopted column densities for Ca II, Ti II, and Mn II. The plot shows a striking underabundance of Ti and Mn in component 3, while their abundance is uniform (at a level of [X/Ca II] ≈ +1.5) throughout the other components. The Ca abundance is low overall, [Ca II/H] ≈ −3.5.

Since the overall metal abundance in the DLA has been constrained to ∼ 0.13 solar (see Sect. 2), the observed abundance pattern in Fig. 3 suggests that all three elements are depleted into dust grains. We note that possible ionization effects, if relevant at these relatively high neutral gas columns, would affect only Ca II and Mn II, but not Ti II, because Ti II and H I have identical ionization potentials (e.g., Morton 2003). The depletion of Ca, Ti, and Mn appears to be > 2 dex in component 3, suggesting that here the dust-to-gas ratio is significantly higher than in the other components. Interestingly, component 3 is also the component with the smallest Doppler parameter, $b = 2.6\,{\rm km\,s^{-1}}$ (Table 1), indicating that the velocity dispersion of the gas in component 3 is small.

Only the second, third, and fourth components show Na I absorption (Fig. A.2). Na I traces cold gas in DLAs at relatively large gas densities (see discussion in Richter et al. 2011) and therefore the detection of Na I possibly indicate an interstellar origin for these components. Although component 3 stands out because of it high dust-to-gas ratio and its narrow absorption, it is not the strongest in Na I, as one might expect intuitively. However, also Na possibly is

depleted into dust grains in such dense interstellar environments, which complicates the interpretation of the observed Na I line strengths.

Component 3, which is narrow and strong in Ca II, weak in Ti II and Mn II, shows all spectral signatures expected for a gaseous disk of a spiral galaxy. This is because in such an environment, one would expect cool, dense gas with a small velocity dispersion and a relatively high dust-to-gas ratio. Since none of the clearly detected galaxies presented in Kacprzak, Murphy & Churchill (2010) lies very close ($\rho <$ 10 kpc) to the quasar sightline or is close in velocity (Fig. 1), and because the metallicity of the DLA is lower than that of the surrounding galaxy population (see Sect. 2), the galaxy disk that gives rise to the absorption in component 3 is possibly related to a faint LSB galaxy that lies in front of PKS 1127−145. This scenario was also preferred by Rao et al. (2003) to explain several low surface-brightness emission features close to the quasar.

The broader and less dust-rich satellite components, in contrast, could well be related to relatively warm, diffuse H I gas from tidal debris due to the interaction between the galaxy-group members, as proposed by Kacprzak et al. (2010). The mild depletion values for Ca and Ti (< 2 dex) in these components are very similar to those found in the Magellanic Stream (Richter et al. 2013), the most nearby tidal gas stream in the Milky Way halo.

4.3. Comparison with other DLAs

In our previous survey of intervening Ti II/Ca II absorbers at low redshift (Guber & Richter 2016), we concluded that the observed abundance of Ca in DLAs and sub-DLAs depends only relatively little on the local metallicity and dust content. Because of the high condensation temperature of Ca ($T_{\rm c} > 1.5 \times 10^3$ K)[3], this element is incorporated into dust grains very efficiently, even at low metallicities and low dust-to-gas ratios. The depletion of Ti in DLAs, in contrast, is much lower in warm, diffuse systems with low-metallicity gas, while it increases dramatically in dense regions with high metallicities. The observed trends for Ti and Ca seen in other absorption-line systems (see compilation by Guber & Richter 2016 and references therein) lead us to the conclusion that the Ti/Ca II ratio in DLAs serves as an excellent tracer for the local dust-to-gas ratio.

A look at Fig. 3 immediately shows that the third component of our DLA has a Ti/Ca II ratio that is substantially lower than in the other absorption components. Indeed, for component 3, we derive [Ti/Ca II] = −0.36, while for the other components, we find [Ti/Ca II] > 1.4. For Mn II, the trend is similar as for Ti II, which will be further discussed in Sect. 5. With [Ti/Ca II] = −0.36, component 3 shows a depletion characteristics that is very similar to the Milky Way disk (Welty & Crowther 2010), while the other components have Ti/Ca II ratios similar to those found in the SMC, LMC, and in other low-redshift DLAs with low metallicities (Guber & Richter 2016).

[3] For a specific element, $T_{\rm C}$ is the temperature below which 50 % of the total amount is condensed into the dust phase (Wasson 1985).

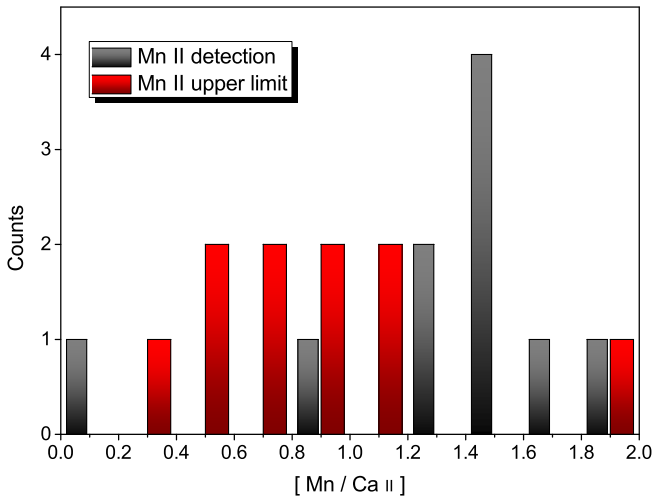


Fig. 4. Mn/Ca II ratios in the six components in the DLA toward PKS 1127−145 and the other DLAs and sub-DLAs studied in Guber & Richter (2016).

5. Mn/Ca II as indicator for the dust-to-gas ratio in DLAs

Figure 3 shows that the depletion of Mn follows that of Ti very closely in the DLA toward PKS 1127−145. In addition, the Mn/Ca II ratio shows a trend that is very similar to that for Ti/Ca II. The question arises whether this trend is typical for DLAs and sub-DLAs and whether the Mn/Ca II ratio could be used as a dust indicator for systems where no Ti information is available.

To further study this interesting aspect, we reinvestigated the Ca II absorbers presented in Richter et al. (2011) and analyzed Mn II absorption in these systems. The results are presented in Table A.3. Only those systems are listed for which a reliable value for log N(Mn II) or an upper limit could be derived.

Generally, the Mn gas phase abundances in these DLAs and sub-DLAs, indeed, seem to closely trace the abundances of Ti, as the three additional Ca II systems with Mn II detections show. The resulting histogram of [Mn/Ca II]-values (Fig. 4), which includes the absorption components of the DLA toward PSK 1127−145 at $z_{\rm abs} =$ 0.313 as individual data points, looks very similar to the histogram for [Ti/Ca II], as presented in Guber & Richter (2016). The Mn II upper limit systems mostly have [Mn/Ca II] < 1.2 while the systems with a measured value for N(Mn II) mostly have larger [Mn/Ca II] ratios. Therefore, similar as for Ti, there seems to be a separation into two classes of absorbers:

1. Class 1: high Mn/Ca II ratios with [Mn/Ca II] > 0.8 and
2. Class 2: low Mn/Ca II ratios with [Mn/Ca II] < 0.8.

As for Ti/Ca II systems, Class 1 Mn/Ca II absorbers trace gas with relatively little dust (Mn only mildly depleted, Ca strongly depleted) while Class 2 systems trace gas with a relatively high dust-to-gas ratio (Mn strongly depleted, similar to Ca).

Also the relation between the Mn II and Ca II column densities in DLAs and sub-DLAs (Fig. 5) is very similar to the one derived for Ti II and Ca II (Guber & Richter (2016); their Fig. 1). Most absorption components of the

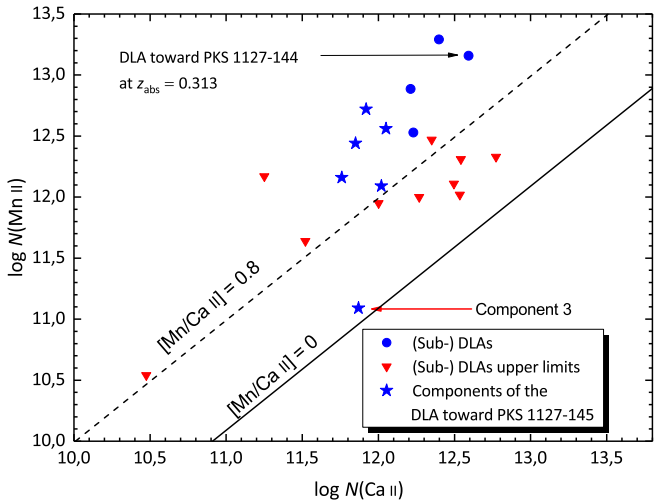


Fig. 5. Relation between column densities of Mn II and Ca II in the DLA toward PKS 1127−145 and other quasar absorption line systems. Only in component 3 of the DLA toward PKS 1127−145, the depletion of Mn into dust grains is as strong as for Ca, so that the resulting [Mn/Ca II] ratio is near the solar value.

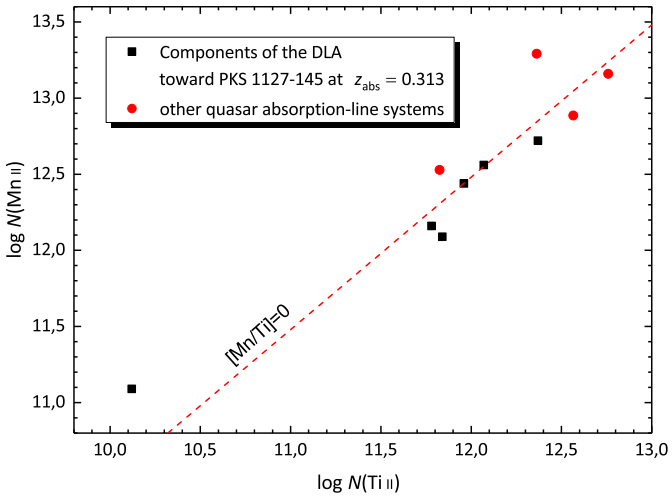


Fig. 6. Relation between Mn II and Ti II for the DLA toward PKS 1127−145 and other quasar absorption-line systems.

DLA toward PKS 1127−145 follow the trend seen in other low-z DLAs while component 3 stands out, having a nearly solar Mn/Ca II ratio.

Beside dust depletion, different nucleosynthetic abundance patterns of elements have influence on their gas-phase abundance ratios. While Ca is an α element and Ti shows an abundance pattern that is similar to the one of an α element (e.g., Welty & Crowther 2010), Mn is an iron-peak element. De Cia et al. (2016) have addressed nucleosynthetic influences on dust depletion measurements in detail. They express that an overabundance of α elments compared to iron-peak elements (short: α enhancement, $\alpha = [\alpha/\mathrm{Fe}]$) is maximal for low-metallicity DLAs, which often have low dust-to-gas-ratios (De Cia et al. 2016). However, possible α enhancements can be expected to be negligible for metal-rich, typically dust-rich, environments, as in molecular clouds in the Milky Way. While De Cia et al. (2016) expect an averaged overabundance of alpha elements compared to Fe of $\alpha_{\max} \approx +0.35$ dex for [Zn/Fe] ≈ 0, for Mn, they find an underabundance of $\alpha_{\max,\mathrm{Mn}} - 0.39$ dex. In fact, in the Class 1 regime, where we expect a comparably low dust-to-gas ratio and low metallicities, the different abundance patterns of Mn and Ca could decrease the Mn/Ca II ratio. Nevertheless, our observations suggest the opposite, indicating that, although the different abundance patterns influence the Mn/Ca II ratio, the effect of dust depletion on the Mn/Ca II ratio is dominating.

The similarity of Mn and Ti as tracers for the dust content in DLAs is further underlined by the trend seen in in Fig. 6. There is a rather tight relation between log N(Mn II) and log N(Ti II) with a slope that is consistent with a solar Mn/Ti ratio, indicating that both ions are similarly sensitive to the local gas phase metal abundance and thus similarly sensitive to the local dust-to-gas ratio.

6. Conclusions

In this paper, we have studied the gas-phase abundances of Ca, Ti, Mn, and Na in the various absorption components of a DLA at $z_{\mathrm{abs}} = 0.313$ toward PKS 1127−145 based on VLT/UVES spectra to explore the dust depletion of these elements and to constrain the origin of the absorber and its components. From previous measurements it is known that the DLA toward PKS 1127−145 is characterized by a complex sub-component structure, a large neutral gas column density (log N(H I) = 21.71), and a relatively low metallicity (~ 0.13 solar).

The following results have been obtained for the DLA:

1. The UVES data imply that the DLA is composed of six major absorption components in Ca, Ti, and Mn, which trace individual neutral gas layers within the DLA. These six components span a velocity range of $\Delta v \approx 140\,\mathrm{km\,s^{-1}}$.
2. We provide high-precision Voigt-profile fits to the individual absorption components and determine column densities (or limits) and Doppler-parameters for Ca II, Ti II, Mn II, and Na I. Assuming a proportionality between N(H I) and N(Ca II), we find that every single sub-component would represent a DLA on its own.
3. Our study indicates a striking underabundance of Ti and Mn in component 3 compared to the other 5 components. The depletion values of Ca, Mn, and Ti in component 3 are >2 dex, suggesting a considerably higher dust-to-gas ratio in this absorption component compared to the other ones. The three inner components (components 2, 3, and 4) are the only ones that show absorption by Na I, indicating the presence for colder and denser gas.
4. Component 3 shows very narrow absorption with a Doppler-parameter b of only 2.6 $\mathrm{km\,s^{-1}}$. It is relatively strong in Ca II, but weak in Ti II and Mn II, pointing toward a large neutral gas column with spatially confined, dense gas that contains substantial amounts of dust. This component therefore shows all signatures of a gaseous disk of a spiral galaxy. These spectral signatures speak for a faint LSB galaxy in front of PKS 1127−145, as the origin for this third component, a scenario that is also preferred by the previous study of Rao et al. (2003).
5. The other, broader and less dust-rich, outer components probably are related to warm, diffuse gas that stems

from tidal debris caused by the interaction between the various galaxy-group members that are associated with the DLA, as proposed by Kacprzak et al. (2010). The relatively mild depletion values for Ca and Ti are very similar to those found in the Magellanic Stream (Richter et al. 2013), the most nearby tidal gas stream in the Milky Way halo.

6. With [Ti/Ca II] = −0.36, component 3 shows depletion characteristics similar to those in the Milky Way disk (Welty & Crowther 2010) while the other components have Ti/Ca II ratios similar to those found in the SMC, LMC, and in other DLAs (Guber & Richter 2016).

From the comparison between the DLA toward PKS 1127−145 and other Ca, Ti, and Mn absorbing environments we draw the following, additional conclusions:

1. A more detailed look into the Mn absorption properties in DLAs suggests that, generally, the Mn II gas-phase abundance seems to be closely related to the gas-phase abundance of Ti II. Following the classification scheme for Ti/Ca II absorption in intervening absorbers presented in Guber & Richter (2016), we suggest that sub-DLAs and DLAs can be subdivided into two classes according to their Mn/Ca II ratio:
   - Class 1: high Mn/Ca II ratios with [Mn/Ca II] > 0.8 and
   - Class 2: low Mn/Ca II ratios with [Mn/Ca II] < 0.8.
2. The tight relation between $\log N$(Mn II) and $\log N$(Ti II) indicates that both ions are similarly sensitive to the local gas-phase metal abundance and thus similarly sensitive to the local dust-to-gas ratio. Therefore, the determination of precise abundances of Ca, Ti, and Mn in low redshift absorption-line systems from optical observations alone may provide important information on the distribution and cross section of dust-rich environments inside and outside of galaxies.

Acknowledgements. Based on observations made with ESO Telescopes at the La Silla Paranal Observatory under programs 67.A-0567(A), 69.A-0371(A), 076.A-0860(A).

References

Asplund, M., Greevese, N., Sauval, A.J., & Scott, P., 2009, arXiv:0909.0948, arxiv.org/abs/0909.0948
Bahcall, J.N. & Spitzer, L.J. 1969, ApJL, 156, L63
Bergeron, J. 1986, A&A, 155, L8
Bergeron, J., & Boissé, P., 1991, A&A, 243, 334
Brüns, C., Kerp, J., & Staveley-Smith, L., 2003, ANS, 324, 80
Chen, H.-W., & Lanzetta, K.M., 2003, ApJ, 597, 796
Chengalur, J.N., & Kanekar, N., 2000, MNRAS, 318, 303
Christensen, L., Møller, P., Fynbo, J.P.U., & Zafar, T. 2014, MNRAS, 445, 225
Chun, M.R., Gharanfoli, S., Kulkarni, V.P., & Takamiya, M., 2006, AJ, 131, 686
De Cia, A., Ledoux, C., Savaglio, S., Schady, P., & Vreeswijk, P.M., 2013, A&A, 560, A88
De Cia, A., Ledoux, C., Mattsson, L., Petitjean, P., Srianand, R., Gavignaud, I., & Jenkins, E.B., 2016, A&A, 596, A97
Dekker, H., D'Odorico, S., Kaufer, A., Delabre, B., & Kotzlowski, H., 2000, Proc. SPIE, 4008, 534
Dessauges-Zavadsky, M., Prochaska, J.X., D'Odorico, S., Calura, F., & Matteucci, F., 2006, A&A, 445, 93
Guber, C.R., & Richter, P., 2016, A&A, 591, A137
Guillemin, P., & Bergeron, J., 1997, A&A, 328, 499
Kanekar, N., Smette, A., Briggs, F.H., & Chengalur, J.N., 2009, ApJ, 705, L40
Kacprzak, G.G., Murphy, T., & Churchill, C.W., 2010, MNRAS, 406, 445
Kacprzak, G.G., Churchill, C.W., Ceverin, D., Steidel, C.C., Klypin, A., & Murphy, M.T., 2010, ApJ, 711, 533
Lane, W., Smette, A., Briggs, F., Rao, S.M., Turnshek, D., & Meylan, G., 1998, AJ, 116, 26
Le Brun, V., Bergeron, J., Boissé, P., & Deharveng, J.M., 1997, A&A, 321, 733
Ledoux, C., Bergeron, J., & Petitjean, P., 2002, A&A, 385, 802
Ledoux, C., Petitjean, P., & Srianand, R., 2003, MNRAS, 346, 209
Morris, S.L. et al. 1993, ApJ, 419, 524
Morton, D.C., 2003, ApJS, 149, 205
Narayanan, A., Misawa, T., Charlton, J.C., & Kim, T.-S., 2007, ApJ, 660, 1093
Nestor, D.B., Rao, S.M., Turnshek, D.A., Monier, E., Lane, W.M., & Bergeron, J., 2002, in *Extragalactic Gas at Low Redshift*, eds. J.S. Mulchaey & J. Stocke J., ASP Conf. Proceedings (San Francisco), 254, 34
Pilyugin, L.S., Grebel, E.K., & Kniazev, A.Y., 2014, AJ, 147, 131
Pilyugin, L.S., Grebel, E.K., Zinchenko, I.A., & Kniazev, A.Y., 2014, AJ, 148, 134
Rao, S.M., & Turnshek, D.A., 2000, ApJS, 130, 1
Rao, S.M., Nestor, D.B., Turnshek, D.A., Lane, W.M., Monier, E.M., & Bergeron, J., 2003, ApJ, 595, 94
Rao, S.M., Belfort-Mihalyi, M., Turnshek, D.A., Monier, E.M., Nestor, D.B., & Quider, A., 2011, MNRAS, 416, 1215
Richter, P., Krause, F., Fechner, C., Charlton, J.C., & Murphy, M.T., 2011, A&A, 528, A12
Richter, P., Fox, A.J., Wakker, B.P., Lehner, N., Howk, J.C., Bland-Hawthorn, J., Ben Bekhti, N., & Fechner, C., 2013, ApJ, 772, 111
Savage, B.D, Sembach, K.R., Tripp, T.M. & Richter, P. 2002, ApJ, 564, 631
Turnshek, D.A. & Rao, S.M., 2002, ApJ, 572, L10
Wasson, J.T., 1985, *Meteorites: Their Record of the Early Solar System History*, Freeman, New York
Welty, D.E., & Crowther, P.A., 2010, MNRAS, 404, 1321

Appendix A: Additional figures and tables

Table A.1. Summary of UVES observations for PKS 1127−145.

setting λ_c (nm)	T_{exp} (s)	Date	Prog.ID
346+580	30,600	2001-05-01,2 / 2001-06-12,13	67.A-0567(A)
390+564	19,200	2002-04-05	69.A-0371(A)
390+580	1,200	2006-01-04	076.A-0860(A)
437+760	1,200	2006-01-04	076.A-0860(A)

Table A.2. Vacuum wavelengths and oscillator strengths for the transitions used in this paper.

Ion & transition	λ_{vac} [Å]	f
Ca II λ3934	3934.7750	0.6267
Ca II λ3969	3969.5901	0.3116
Mn II λ2576	2576.877	0.361
Mn II λ2594	2594.499	0.280
Mn II λ2606	2606.462	0.198
Na I λ5891	5891.5833	0.640
Na I λ5897	5897.5581	0.3201
Ti II λ3073	3073.863	0.121
Ti II λ3242	3242.918	0.232
Ti II λ3384	3384.730	0.358

References. All data are from Morton (2003).

Table A.3. Column densities of H I, Ca II, Ti II, and Mn II for DLAs and sub-DLAs from the sample of Guber & Richter (2016).

QSO-sightline	$z_{\rm abs}$	$\log N$(H I)	$\log N$(Ca II)	$\log N$(Ti II)	$\log N$(Mn II)
J095456+174331	0.23782	21.32[a]	12.21±0.03	12.57±0.05	12.89±0.05
J113007−144927*	0.31271	21.71[b]	12.59±0.02	12.76±0.04	13.16±0.02
J123200−022404	0.39498	20.6[c]	12.40±0.02	12.36±0.05	13.29±0.02
J045608−215909	0.47439	19.5[d]	12.23±0.02	11.83±0.05	12.53±0.02
Additional Ca II systems with upper limits for N(Mn II)					
J124646−254749	0.49282	–	12.77±0.08	< 11.93	< 12.33
J220743−534633	0.43720	–	12.00±0.07	< 11.50	< 11.95
J051707−441055	0.42913	–	10.48±0.06	< 10.20	< 10.54
J232820+002238	0.41277	–	11.52±0.08	< 11.14	< 11.64
J224752−123719	0.40968	–	12.27±0.04	< 11.34	< 12.00
J050112−015914	0.40310	–	12.35±0.05	< 12.08	< 12.47
J110325−264515	0.35896	–	11.25±0.04	< 10.55	< 12.17
J142253−000149	0.34468	–	12.35±0.05	< 11.88	< 12.02
J231359−370446	0.33980	–	12.54±0.03	< 12.19	< 12.31
J102837−010027	0.32427	–	12.50±0.03	< 11.68	< 12.11

Notes. * This absorption line system is the multicomponent DLA toward PKS 1127−144 at $z_{\rm abs} = 0.31271$ studied in this paper. The given column densities for this absorber (for Ca II, Ti II, and Mn II), each, are summed over the six components as given in the last row of Table 1.

References. (a) Rao et al. (2003); (b) Lane et al. (1998); (c) Le Brun et al. (1996); (d) Turnshek & Rao (2002).

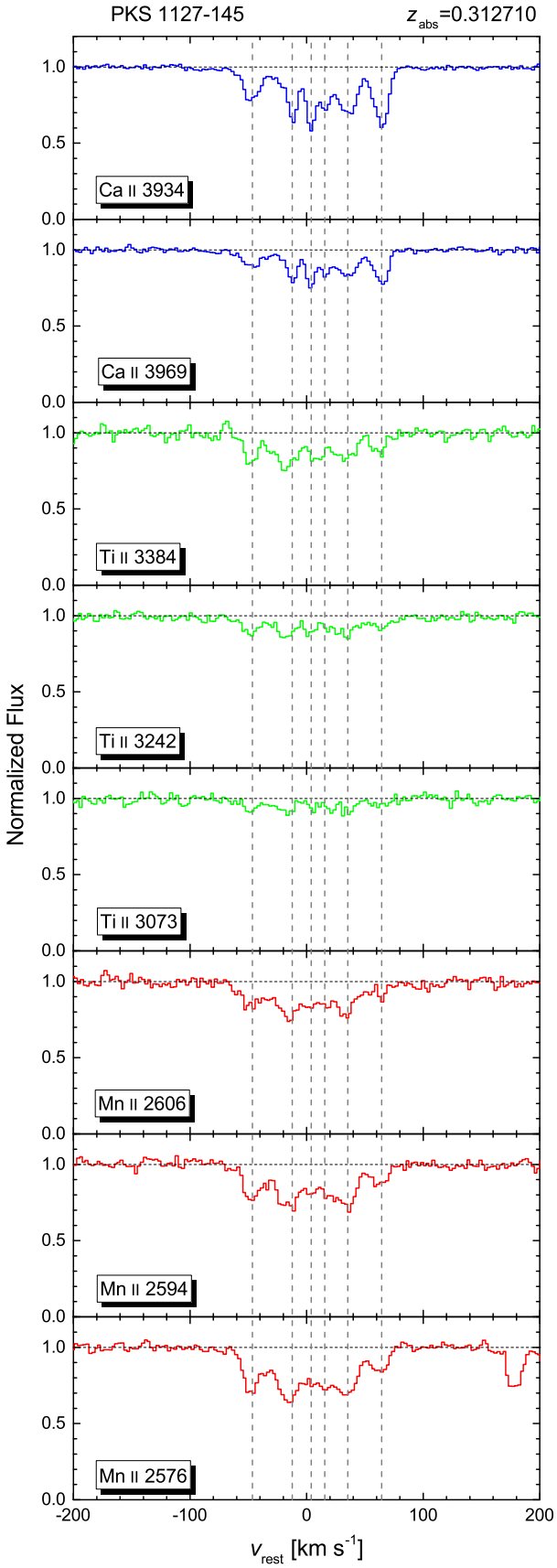


Fig. A.1. Velocity profiles for various transitions of Ca II, Ti II, and Mn II in the $z_{\rm abs} = 0.313$ DLA toward PKS 1127−145 based on archival VLT/UVES data.

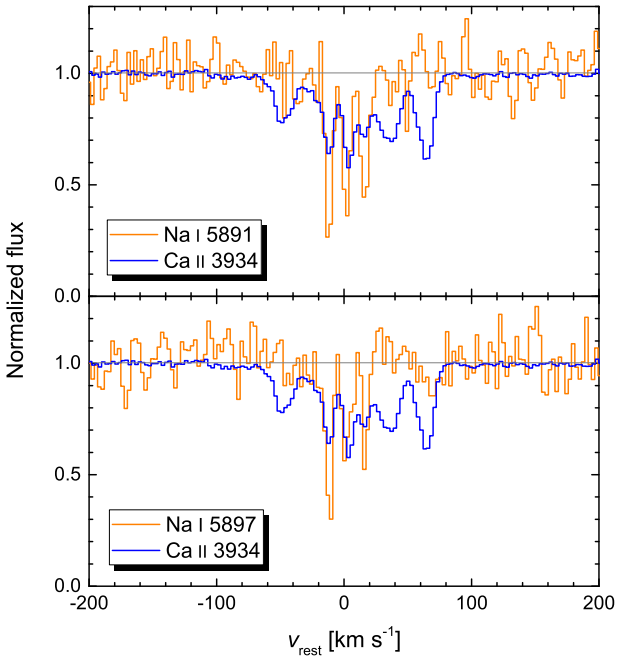


Fig. A.2. Velocity profiles of Na I and Ca II toward PKS 1127−145 at $z_{\rm abs} = 0.313$. Only in components 2, 3, and 4, Na I absorption is detected.